






Reovirus Nonstructural Protein σ NS Recruits Viral RNA to Replication Organelles

Christopher H. Lee,^{a,b}  Krishnan Raghunathan,^{b,c} Gwen M. Taylor,^{b,c} Andrea J. French,^a Raquel Tenorio,^d Isabel Fernández de Castro,^d Cristina Risco,^d  John S. L. Parker,^e  Terence S. Dermody^{a,b,c}

^aDepartment of Microbiology and Molecular Genetics, University of Pittsburgh School of Medicine, Pittsburgh, Pennsylvania, USA

^bInstitute of Infection, Inflammation, and Immunity, University of Pittsburgh Medical Center Children's Hospital of Pittsburgh, Pittsburgh, Pennsylvania, USA

^cDepartment of Pediatrics, University of Pittsburgh School of Medicine, Pittsburgh, Pennsylvania, USA

^dCell Structure Laboratory, National Center for Biotechnology, CNB-CSIC, Madrid, Spain

^eBaker Institute for Animal Health, College of Veterinary Medicine, Cornell University, Ithaca, New York, USA

ABSTRACT The function of the mammalian orthoreovirus (reovirus) σ NS nonstructural protein is enigmatic. σ NS is an RNA-binding protein that forms oligomers and enhances the stability of bound RNAs, but the mechanisms by which it contributes to reovirus replication are unknown. To determine the function of σ NS-RNA binding in reovirus replication, we engineered σ NS mutants deficient in RNA-binding capacity. We found that alanine substitutions of positively charged residues in a predicted RNA-binding domain decrease RNA-dependent oligomerization. To define steps in reovirus replication facilitated by the RNA-binding property of σ NS, we established a complementation system in which wild-type or mutant forms of σ NS could be tested for the capacity to overcome inhibition of σ NS expression. Mutations in σ NS that disrupt RNA binding also diminish viral replication and σ NS distribution to viral factories. Moreover, viral mRNAs only incorporate into viral factories or factory-like structures (formed following expression of nonstructural protein μ NS) when σ NS is present and capable of binding RNA. Collectively, these findings indicate that σ NS requires positively charged residues in a putative RNA-binding domain to recruit viral mRNAs to sites of viral replication and establish a function for σ NS in reovirus replication.

IMPORTANCE Viral replication requires the formation of neorganelles in infected cells to concentrate essential viral and host components. However, for many viruses, it is unclear how these components coalesce into neorganelles to form factories for viral replication. We discovered that two mammalian reovirus nonstructural proteins act in concert to form functioning viral factories. Reovirus μ NS proteins assemble into exclusive factory scaffolds that require reovirus σ NS proteins for efficient viral mRNA incorporation. Our results demonstrate a role for σ NS in RNA recruitment to reovirus factories and, more broadly, show how a cytoplasmic non-membrane-enclosed factory is formed by an RNA virus. Understanding the mechanisms of viral factory formation will help identify new targets for antiviral therapeutics that disrupt assembly of these structures and inform the use of nonpathogenic viruses for biotechnological applications.

KEYWORDS reovirus, σ NS, μ NS, viral RNA-binding proteins, viral factories, viral genetics

Viral factories are intracellular structures formed during infection that promote production of progeny virions. These neorganelles concentrate viral and host components to establish discrete intracellular environments that are optimal for viral genome replication, packaging, and often immune evasion or suppression (1). While it is known that factories require viral proteins and RNAs, mechanisms by which these viral

Citation Lee CH, Raghunathan K, Taylor GM, French AJ, Tenorio R, Fernández de Castro I, Risco C, Parker JSL, Dermody TS. 2021. Reovirus nonstructural protein σ NS recruits viral RNA to replication organelles. *mBio* 12:e01408-21. <https://doi.org/10.1128/mBio.01408-21>.

Editor Stacy M. Horner, Duke University Medical Center

Copyright © 2021 Lee et al. This is an open-access article distributed under the terms of the [Creative Commons Attribution 4.0 International license](https://creativecommons.org/licenses/by/4.0/).

Address correspondence to Terence S. Dermody, terence.dermody@chp.edu.

Received 17 May 2021

Accepted 28 May 2021

Published 6 July 2021

components are recruited and concentrated are not well understood, especially for viruses that contain double-stranded (ds) RNA genomes.

Mammalian orthoreovirus (reovirus) has been implicated in the development of celiac disease (2) and is being investigated as an oncolytic therapeutic (3). Mature reovirus virions package 10 unique segments of dsRNA in two concentric shells, termed outer capsid and core (4). Following reovirus internalization into the endocytic compartment, the outer capsid is proteolytically removed, allowing penetration of the viral core into the cytoplasm (5). The core transcribes viral mRNAs that are translated by host ribosomes. Newly synthesized viral proteins reorganize the cytoplasm, establishing dynamic factories (6, 7) embedded in a matrix of membranes derived from the endoplasmic reticulum (6–8). Formation of these reovirus replication organelles requires two nonstructural proteins, μ NS and σ NS, which are expressed at early stages of infection (9). As infection progresses, additional viral replication components are concentrated in the factories, increasing their size (10). How these essential viral components are recruited to factories is not well defined.

The μ NS protein forms the scaffold for reovirus factories (11). Expression of μ NS in cells leads to the formation of dynamic globular structures that resemble liquid-liquid phase-separated condensates (7, 12). These structures do not require other reovirus proteins to form and appear similar in morphology to reovirus factories (9). As such, μ NS puncta in uninfected cells are called factory-like structures (13). Protein components of reovirus cores are recruited to factory-like structures when coexpressed with μ NS, suggesting that μ NS concentrates reovirus proteins essential for viral assembly (14).

The σ NS protein is a single-stranded (ss) RNA-binding protein that distributes diffusely in the cytoplasm when expressed alone but localizes to factory-like structures in the presence of μ NS (9). Recruitment of σ NS to μ NS puncta requires the N-terminal regions of both proteins (15). Purified σ NS interacts preferentially with ssRNAs and does not display sequence specificity (16). It is not known whether σ NS binds ssRNA nonspecifically in infected cells. However, σ NS can immunoprecipitate all 10 viral mRNAs from reovirus-infected cells and protects specific regions of viral mRNAs from degradation (17, 18). The N-terminal 38 residues of σ NS are required for RNA binding (19), suggesting that this region forms an RNA-binding domain, although the mechanism by which σ NS binds RNA and the function of its RNA-binding capacity in viral replication are unknown. Since this reovirus protein binds ssRNAs and localizes to viral factories, we hypothesized that it recruits viral mRNAs to these organelles.

In this study, we identified residues required for σ NS binding to ssRNA by using targeted mutagenesis and found that these residues are required for efficient reovirus replication. Additionally, we discovered that viral mRNAs localize to viral factories and factory-like structures only when wild-type (WT) σ NS is present. Collectively, our findings suggest that a function of the enigmatic σ NS protein is to act in concert with μ NS to recruit viral mRNAs to sites of viral replication.

RESULTS

Engineering σ NS mutants deficient in RNA binding. To determine whether the RNA-binding capacity of σ NS is required for reovirus replication, we engineered σ NS mutants deficient in binding RNA. The first 38 residues in the σ NS N terminus (Fig. 1A) are required for binding to RNA *in vitro* (19). These residues are conserved in available σ NS sequences (20), and three of these residues (R6, R14, and R29) are conserved in σ NS proteins of other *Orthoreovirus* species (see Fig. S1 in the supplemental material). Protein-RNA contacts occur by electrostatic or base-stacking interactions (21), and approximately 25% of the residues in this region of σ NS are capable of mediating both types of interactions. We hypothesized that disrupting electrostatic or base-stacking interactions would prevent σ NS from binding RNA. To test this hypothesis, we engineered seven alanine substitution mutations individually into a σ NS expression plasmid, resulting in seven σ NS mutants (R6A, K11A, R14A, Y25A, R29A, K35A, and R38A).

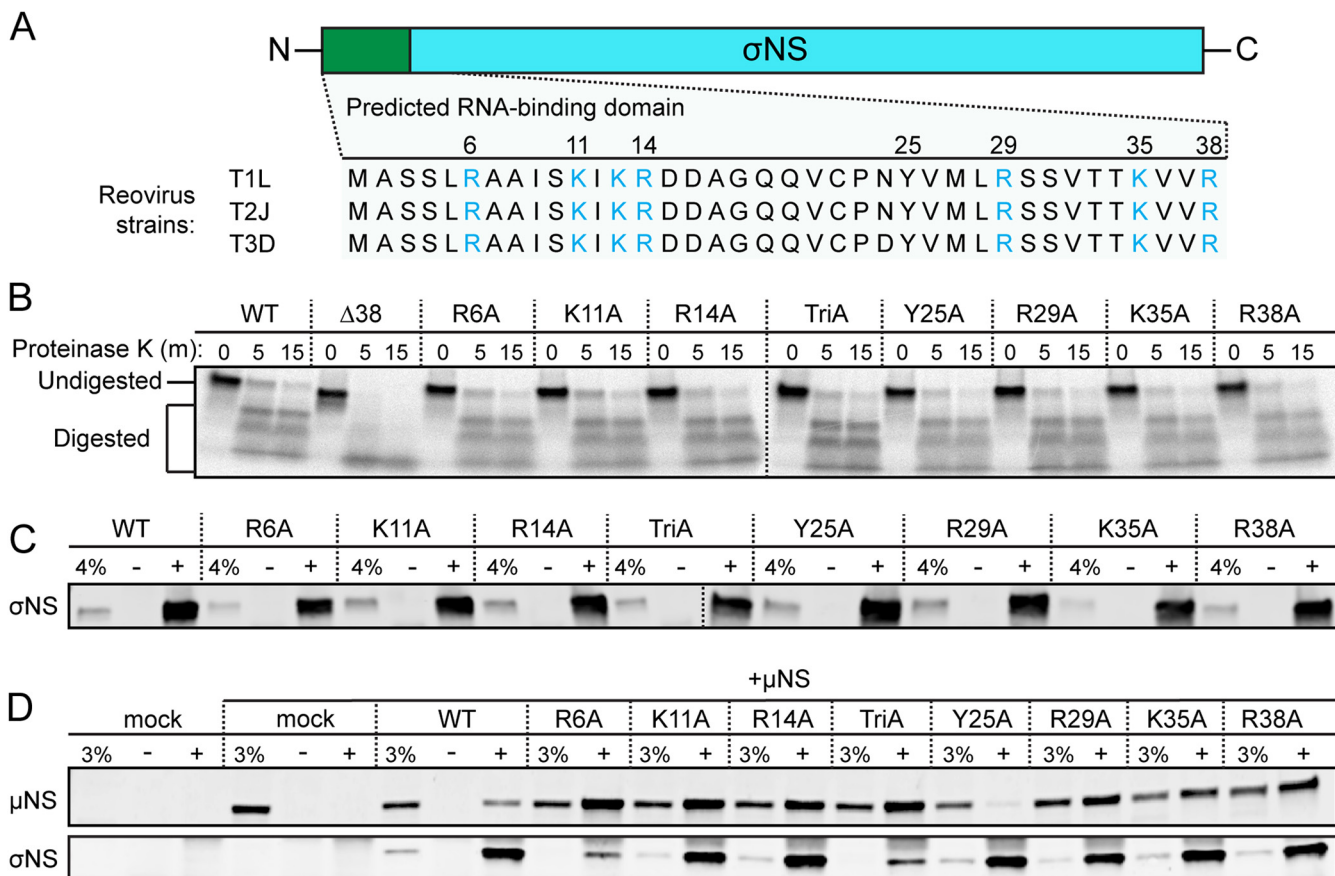


FIG 1 Mutations in σ NS do not appear to alter protein folding. (A) Sequence alignment of the N-terminal 38 amino acids (green bar) of σ NS encoded by mammalian reovirus strains T1L, T2J, and T3D. Positively charged residues are shown in blue. (B) 35 S-labeled *in vitro*-expressed σ NS was incubated with proteinase K for the times shown, resolved by SDS-PAGE, and visualized by autoradiography. HEK293T cells were transfected with σ NS alone (C) or cotransfected with σ NS and μ NS (D) and incubated for 24 h. Total protein in cell lysates was immunoprecipitated using an IgG isotype antibody (–), conformation-specific σ NS-specific monoclonal antibody 2A9 (C; +), or σ NS-specific monoclonal antibody 3E10 (D; +), resolved by SDS-PAGE, and immunoblotted using antisera directed against σ NS (C and D) or μ NS (D). Percentages of total lysates in the immunoprecipitation reactions (4% [C] or 3% [D]) were used as loading controls.

We also engineered a triple mutant to disrupt a cluster of positively charged residues in the N terminus (K11A, K13A, and R14A; termed TriA) and a mutant lacking the N-terminal 38 residues (Δ 38).

To verify that the engineered σ NS mutations do not disrupt protein folding, we characterized the mutants using three independent approaches. First, we conducted limited proteolysis of WT and mutant σ NS proteins recovered from coupled *in vitro* transcription and translation reactions using rabbit reticulocyte lysates supplemented with 35 S methionine. Following *in vitro* expression, WT and mutant proteins were digested with proteinase K, and digestion reactions were resolved by polyacrylamide gel electrophoresis (PAGE) (Fig. 1B). The only mutant that differed from WT σ NS in digestion kinetics or resultant protein fragments was Δ 38 σ NS. Based on these results, we concluded that Δ 38 σ NS is not properly folded and excluded this mutant from subsequent analyses. Second, we used σ NS conformation-specific monoclonal antibody 2A9 (10) to immunoprecipitate σ NS expressed in HEK293T cells (Fig. 1C). While various levels of protein expression were apparent, all of the mutants were immunoprecipitated by this conformation-specific antibody, suggesting that the mutations do not disrupt an epitope in σ NS recognized by this antibody. Third, we tested whether the mutant σ NS proteins were capable of co-immunoprecipitation (co-IP) with a known σ NS-binding partner, reovirus μ NS protein. The two proteins were coexpressed in HEK293T cells, and co-IPs were conducted using monoclonal antibody 3E10, which also is directed against σ NS (10) (Fig. 1D). Each of the mutants was capable of

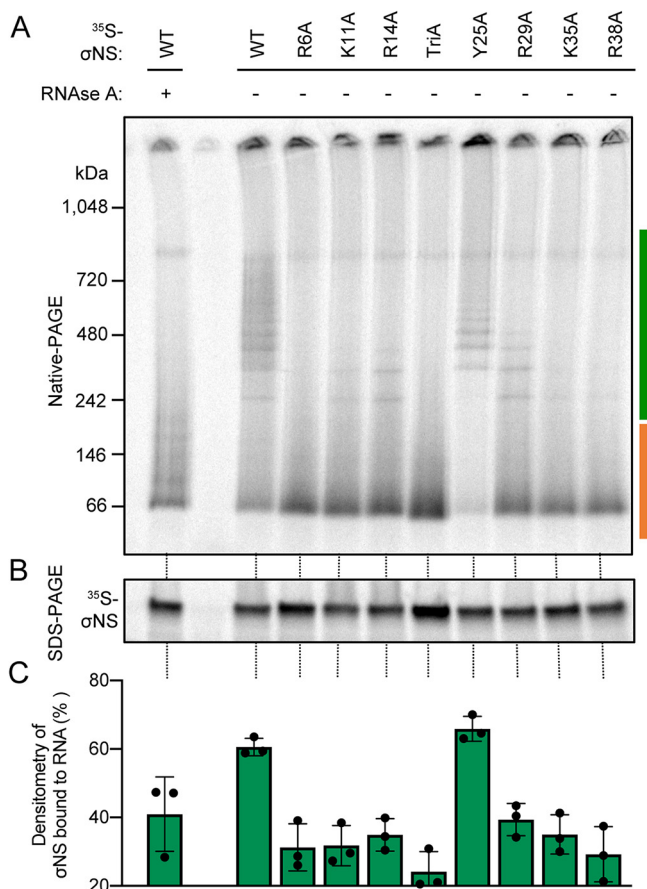


FIG 2 Alanine substitution of positively charged residues in a predicted RNA-binding domain of σ NS alters RNA-dependent oligomerization. ^{35}S -labeled σ NS was expressed in rabbit reticulocyte lysates (RRLs) and incubated with or without RNase A. Samples were resolved by native PAGE to preserve oligomeric species (A) or SDS-PAGE to monitor protein expression (B) and visualized by autoradiography. The scale bar to the left of the native polyacrylamide gel (A) marks the kilodalton (kDa) ranges used for densitometric analysis of each σ NS construct. The green scale bar marks σ NS bound to RNA, whereas the orange scale bar marks unbound σ NS. (C) The efficiency with which each σ NS construct forms RNA-dependent oligomers was calculated by dividing the density of σ NS bound to RNA (panel A, green scale bar) by the total density of σ NS present in the gel (panel A, green and orange scale bar).

immunoprecipitating μ NS. Surprisingly, replacing positively charged residues in σ NS with alanine residues promoted more efficient immunoprecipitation of μ NS. Collectively, the σ NS alanine substitutions and the TriA σ NS mutant yielded folding phenotypes comparable to that of WT σ NS and were capable of interacting with a known σ NS-binding partner, suggesting that the mutations do not substantially alter σ NS structure.

We next evaluated the RNA-binding capacity of the σ NS mutants using an RNA-dependent electrophoretic mobility shift assay (EMSA). In these experiments, we employed a property of σ NS to form oligomeric ladders with RNA when expressed *in vitro* (19). These ladders collapse following treatment with RNase A (Fig. 2A), indicating that RNA binding is required for ladder formation. WT and mutant σ NS proteins were expressed in rabbit reticulocyte lysates in the presence of ^{35}S methionine. Half of each protein sample was resolved using native PAGE to separate complexes of σ NS and RNA, while the other half was electrophoresed using denaturing PAGE to compare protein levels (Fig. 2B). Based on the molecular weight of monomeric WT σ NS (~ 37 kDa), σ NS appears to migrate in the presence of RNA as a hexamer and correspondingly larger species that vary by two monomers of σ NS each. Treatment of the σ NS-RNA complexes with RNase A yielded a band that migrates at approximately the 66-kDa-

molecular-weight marker, which likely represents a dimer of σ NS not bound to RNA. Mutant forms of σ NS produced bands that migrated at comparable molecular weights to the dimer, but the intensities varied, inversely correlating with the intensities of the higher-molecular-weight bands. The percentage of RNA-dependent oligomers for each σ NS protein was determined by dividing the total density of bands migrating between ~200 and 1,000 kDa (Fig. 2A, green bar) by the sum of the densities of all bands observed in the gel (Fig. 2A, green and orange bars). Two mutants, R6A and TriA σ NS, did not display any detectable RNA-dependent oligomerization (Fig. 2A). The RNA-binding capacity of the other charged-to-alanine mutants was less than that of WT or Y25A σ NS (Fig. 2C). However, all σ NS-RNA complexes were sensitive to RNase A treatment. Most mutants yielded dominant dimer bands following RNase A treatment, but the Y25A mutant did not. Instead, Y25A σ NS appeared to aggregate at the top of the gel following RNase A treatment (see Fig. S2). These results suggest that positively charged residues in the σ NS N terminus are required for RNA binding. However, predicted base-stacking interactions mediated by Y25 appear dispensable for this property, but without RNA, the Y25A mutant appeared more prone to aggregation.

Mutants of σ NS incapable of RNA binding fail to complement σ NS knockdown during infection. To test whether σ NS RNA-binding capacity contributes to reovirus replication, we first attempted to recover reoviruses encoding the R6A, K11A, or R29A mutations in σ NS using reverse genetics. Plaque-forming mutant viruses were not recovered in three independent attempts, suggesting that residues required for RNA binding are also required for viral replication. To define the step in reovirus replication facilitated by the RNA-binding capacity of σ NS, we established a complementation system in which WT or mutant forms of the proteins could be tested for the capacity to overcome inhibition of σ NS expression. First, we evaluated the capacity of expressed WT or mutant σ NS proteins to complement σ NS knockdown in HEK293T cells constitutively expressing σ NS-specific small interfering RNAs (σ NS-siRNA cells) (19). As a control, we used HEK293T cells constitutively expressing siRNAs directed against green fluorescent protein (GFP-siRNA cells) (19). We transfected these cells with expression plasmids encoding GFP as a negative control, WT σ NS, or σ NS incorporating synonymous mutations in the siRNA recognition site (σ NS mismatch [σ NS-MM]). Transfected cells were incubated for 24 h, after which time, cells were adsorbed with reovirus at a low multiplicity of infection (MOI). We used a low MOI in these experiments to enable the constitutively expressed siRNAs to diminish the expression of virus-encoded σ NS transcripts. As anticipated, at 24 h postadsorption, σ NS protein levels (Fig. S3A) and reovirus replication (Fig. S3B) were unaffected by the GFP-restricting siRNA. However, σ NS protein expression was not detected and reovirus replication was substantially impaired by the σ NS-restricting siRNA, and neither σ NS expression nor reovirus replication was complemented by GFP. σ NS protein expression was greater following σ NS-MM transfection relative to that following WT σ NS transfection (Fig. S3A), demonstrating the susceptibility of WT σ NS transcripts to siRNA-mediated knockdown in these cells. However, transfection of WT σ NS into reovirus-infected σ NS-siRNA cells allowed reovirus yields to reach levels comparable to those following transfection of σ NS MM, indicating that increased levels of σ NS allowed by the mismatch mutations in the siRNA target sequence do not lead to increased production of viral progeny (Fig. S3B). Both WT and MM σ NS were capable of promoting reovirus replication in σ NS-siRNA cells relative to that for complementation with GFP. These results indicate that overexpression of σ NS prior to infection can rescue reovirus replication in cells expressing σ NS-specific siRNAs and that rescue is independent of mismatch mutations in the σ NS siRNA target sequence.

To determine whether the engineered σ NS mutants can complement reovirus replication in cells expressing σ NS-specific siRNAs, we transfected GFP-siRNA and σ NS-siRNA cells with the σ NS mutants, adsorbed with reovirus, and monitored viral yields by plaque assay (Fig. 3A). Following infection of GFP-siRNA cells, viral yields were only modestly altered by expression of WT or mutant σ NS (Fig. 3B). In contrast, following infection of σ NS-siRNA cells, viral yields were reduced to a maximum of 10,000-fold

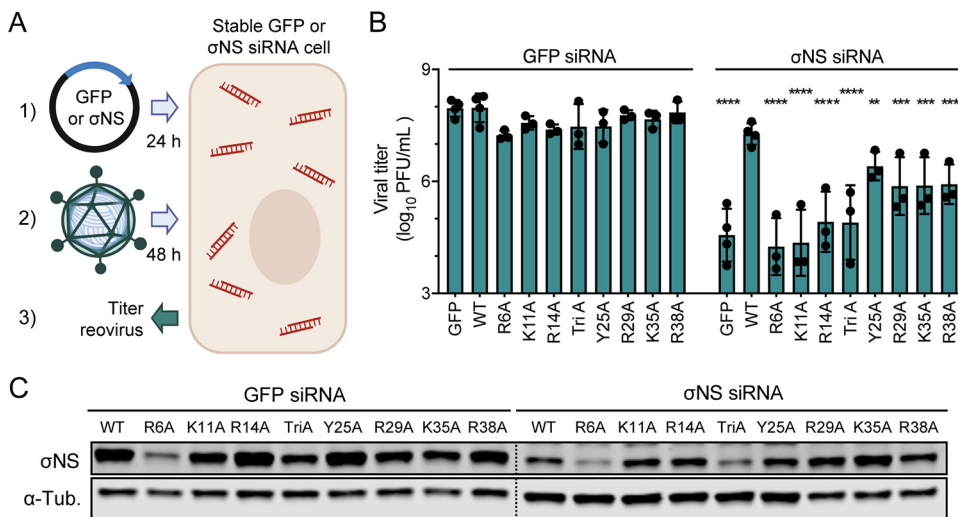


FIG 3 Mutants of σ NS incapable of RNA binding fail to complement reovirus replication in cells expressing σ NS-specific siRNAs. (A) Cells that constitutively express siRNAs directed against GFP or σ NS were transfected with expression plasmids encoding GFP or the σ NS constructs shown and incubated for 24 h. Cells were adsorbed with reovirus strain T3D at an MOI of 5 PFU/cell and incubated for 48 h. (B) Cell culture supernatants were collected for infectious virus quantification by plaque assay. Titer values that differ significantly from those obtained from cells expressing siRNAs against GFP complemented with GFP by one-way ANOVA with Dunnett's multiple-comparison test are shown. **, $P < 0.0021$; ***, $P < 0.0002$; ****, $P < 0.0001$. (C) Cells that constitutively express siRNAs against GFP or σ NS were transfected with expression plasmids encoding the σ NS constructs shown and incubated for 24 h. Cell lysates were resolved by SDS-PAGE and immunoblotted using antisera directed against σ NS and monoclonal antibodies specific for alpha-tubulin (α -Tub). Panel A was prepared using BioRender.

following expression of the σ NS mutants incapable of binding RNA relative to expression of WT σ NS (Fig. 3B). Additionally, Y25A σ NS complemented reovirus replication more efficiently than the other mutants, albeit at lower levels than WT σ NS. Transfection of GFP-siRNA and σ NS-siRNA cells with σ NS mutants resulted in variable levels of σ NS protein after 24 h of incubation (Fig. 3C). R6A σ NS and TriA σ NS displayed the lowest levels of expression, which was surprising, as expression of these mutants was similar to that of WT σ NS in rabbit reticulocyte lysates (Fig. 2B). However, levels of σ NS present prior to infection did not correlate with the capacity of the mutants to complement σ NS siRNA-mediated knockdown (Fig. 3B). K11A σ NS, which was expressed at levels comparable to WT σ NS, and R14A σ NS, which was expressed at higher levels than WT σ NS, were incapable of restoring viral replication. These results suggest that the capacity of σ NS to support viral replication is not strictly contingent on levels of σ NS expression but instead on properties of the protein that were altered following mutagenesis, likely, the capacity to bind RNA.

σ NS incorporation into reovirus factories is disrupted by mutations that alter RNA binding. In reovirus-infected cells, σ NS preferentially localizes to viral factories (10). To determine whether σ NS distribution in cells contributes to its function, we assessed the intracellular distribution of WT and mutant forms of σ NS during infection. We selected three mutants (R6A, Y25A, and R29A) to represent our panel of σ NS mutants in this and subsequent experiments. The R6A and R29A mutants displayed little to no RNA-dependent oligomerization and failed to complement σ NS knockdown in infected σ NS-siRNA cells (Fig. 3B). The Y25A mutant displayed RNA-dependent oligomerization comparable to that of WT σ NS and complemented σ NS knockdown in infected σ NS-siRNA cells more efficiently than the other σ NS mutants. To evaluate the distribution of mutant σ NS during infection, we transfected σ NS-siRNA cells with WT or mutant forms of σ NS, infected them with reovirus, stained them with antibodies specific for σ NS and μ NS, and imaged the cells using confocal immunofluorescence microscopy (Fig. 4A). Viral factory structures were demarcated by intense μ NS staining. Factories formed under all conditions tested and retained a globular morphology,

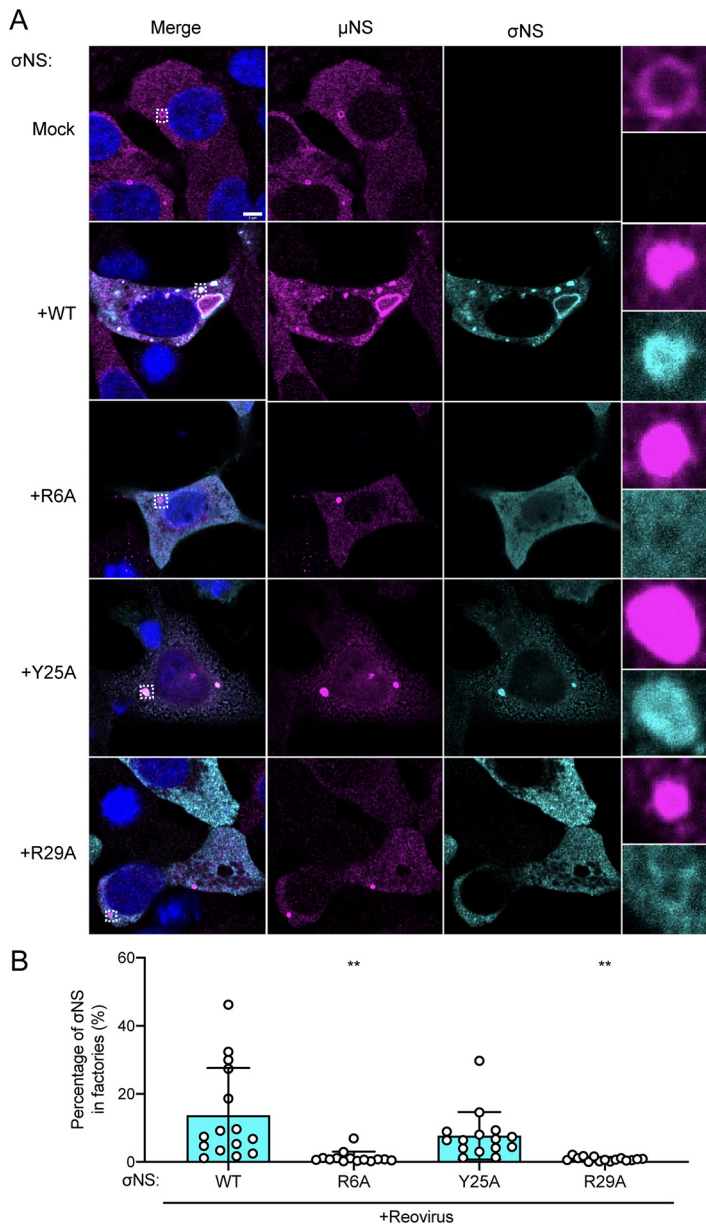


FIG 4 Mutations in σ NS that compromise RNA binding disrupt incorporation of the protein into reovirus replication organelles. (A) Cells that constitutively express siRNAs directed against σ NS were transfected with expression plasmids encoding the σ NS constructs shown and incubated for 24 h. Cells were adsorbed with reovirus strain T3D at an MOI of 5 PFU/cell, incubated for 48 h, fixed, stained using σ NS-specific monoclonal antibody 3E10 (cyan), μ NS-specific antiserum (magenta), and DAPI (blue), and imaged using confocal microscopy. Regions selected for magnification are indicated by dotted white boxes. Bar, 5 μ m. (B) The percentage of σ NS immunofluorescence signal in reovirus factories was quantified by dividing the sum of σ NS signal in reovirus factories by the sum of cytoplasmic σ NS signal. Individual data points represent single cells. Percentage values that differ significantly from those obtained from WT σ NS-transfected reovirus-infected cells by one-way analysis of variance (ANOVA) with Dunnett’s multiple-comparison test are shown. **, $P < 0.0021$.

which is characteristic of the type 3 Dearing (T3D) strain of reovirus used in these experiments (22). However, factories formed in the absence of σ NS expression or in the presence of the R6A or R29A σ NS mutants were smaller than those formed in the presence of WT or Y25A σ NS. Immunofluorescence signals for WT and Y25A σ NS were more frequently detected in viral factories, while those produced by the R6A and R29A σ NS mutants were more frequently detected outside viral factories (Fig. 4B).

Collectively, these observations suggest that mutations impairing RNA binding limit viral factory maturation and alter σ NS distribution to viral factories.

To confirm that the preferential distribution of σ NS to the periphery of larger viral factories was not solely due to poor penetration of σ NS-specific antibodies into factories of fixed and permeabilized cells, we processed reovirus-infected cells for Tokuyasu cryosections, stained σ NS with gold-labeled σ NS-specific antibodies, and imaged the cells using transmission electron microscopy (Fig. S4). Small puncta containing σ NS were observed throughout the cytoplasm in the majority of infected cells. These small puncta were not coated at the periphery with σ NS, and instead, σ NS was distributed diffusely in these structures (Fig. S4A and B). However, in larger electron-dense factories, σ NS was concentrated at the factory periphery (Fig. S4C and D), consistent with previous results (23). These observations suggest that σ NS distributes to the factory periphery as these structures enlarge.

To determine whether incorporation of σ NS into reovirus factories depends on viral replication, we used a simplified factory-like structure model system (9, 11). We transfected HEK293T cells with μ NS and WT or mutant forms of σ NS and processed the cells for confocal immunofluorescence microscopy to visualize σ NS and μ NS (Fig. 5A). WT and Y25A σ NS were efficiently incorporated into factory-like structures (Fig. 5B). The morphology and size of these structures resembled those of viral factories observed during reovirus infection (Fig. 5B). In contrast, the R6A and R29A σ NS mutants were poorly incorporated into factory-like structures (Fig. 5B) and recapitulated phenotypes observed during complementation of reovirus-infected cells (Fig. 4B). Based on data presented thus far, we conclude that RNA promotes oligomerization of σ NS, which could enable a greater number of σ NS molecules to incorporate into factory structures, overcoming saturation limits of μ NS binding.

Mutations in σ NS that alter RNA binding diminish mRNA incorporation in reovirus factories. Since the R6A and R29A σ NS mutants are altered in RNA binding and incorporation into viral factories, we hypothesized that viral mRNAs also are mislocalized in infected σ NS-siRNA cells transfected with these mutants. To test this hypothesis, we transfected σ NS-siRNA cells with WT or mutant forms of σ NS, infected them with reovirus, and processed the cells 48 h postadsorption for fluorescence *in situ* hybridization (FISH) coupled with immunofluorescence detection of μ NS to visualize reovirus factories (Fig. 6A). FISH probes were designed to specifically detect either the reovirus σ NS-encoding mRNA (σ NS mRNA) or the reovirus σ 3-encoding mRNA (σ 3 mRNA), which encodes outer-capsid protein σ 3. Following infection of σ NS-siRNA cells by reovirus, viral mRNAs were not detected in viral factories. Expression of WT and Y25A σ NS prior to infection led to the formation of larger viral factories than in untransfected cells, and importantly, both σ NS and σ 3 mRNAs were detected in cells. Interestingly, σ 3 mRNAs were not concentrated in factories to the same extent as σ NS mRNAs, but both σ NS and σ 3 mRNAs were observed to colocalize in discrete high-intensity puncta in viral factories, suggesting a suborganization in the factory structures. While expression of WT and Y25A σ NS promoted conditions to allow detection of viral mRNAs in factories, expression of the R6A and R29A σ NS mutants did not. R6A and R29A σ NS mRNAs were detected in cells containing small factories, but these mRNAs were not observed in the factory structures. These results suggest that viral mRNAs are not efficiently produced or do not distribute to factories when σ NS is incapable of interacting with RNA.

We were surprised that σ 3 mRNAs were not concentrated in functioning factories to the same extent as σ NS mRNAs. We hypothesized that differences in σ NS and σ 3 mRNA localization could be dependent on the time point at which we fixed cells for imaging. To test this hypothesis, we infected HEK293T cells with reovirus, and processed the cells at 9, 24, and 48 h postadsorption for FISH coupled with immunofluorescence detection of μ NS to visualize reovirus factories (Fig. S5). Both σ 3 and σ NS mRNAs were concentrated in factories at 9 and 24 h postadsorption. However, at 48 h postadsorption, σ 3 mRNAs distributed less prevalently to factories, while σ NS mRNAs

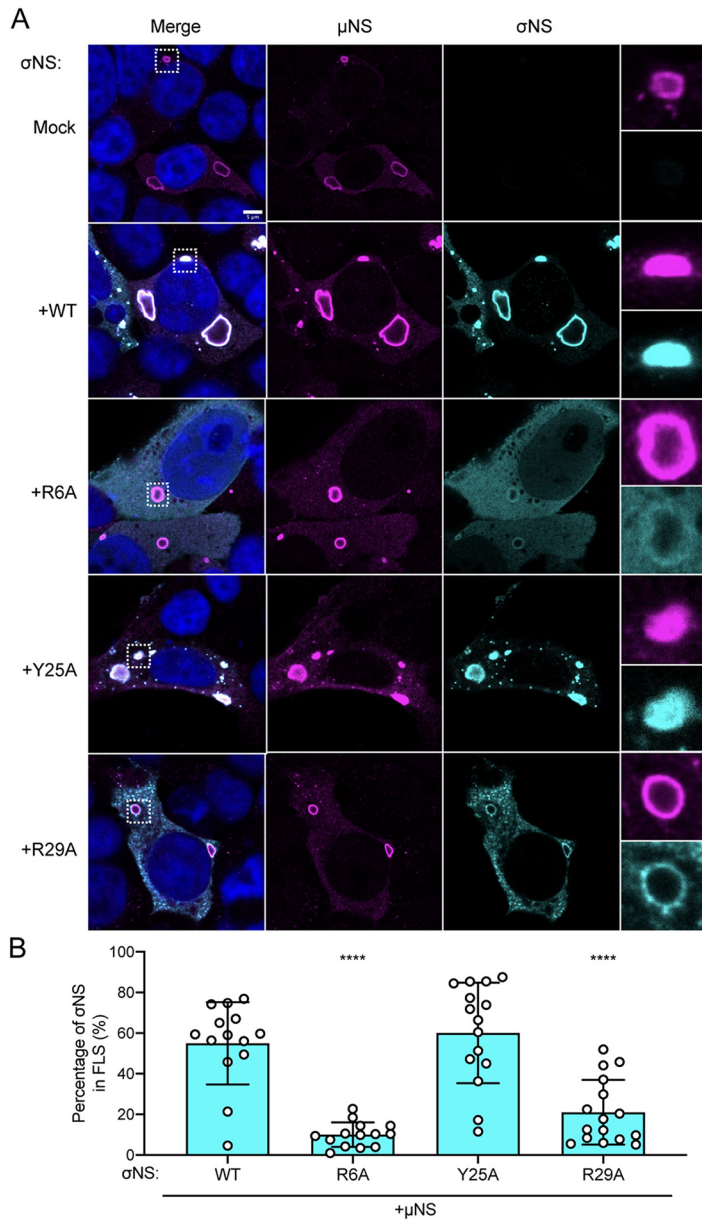


FIG 5 Mutations in σ NS that compromise RNA binding disrupt incorporation of the protein into factory-like structures. (A) Cells were transfected with expression plasmids encoding the σ NS constructs shown along with μ NS and incubated for 24 h. Cells were fixed, stained using σ NS-specific monoclonal antibody 3E10 (cyan), μ NS-specific antiserum (magenta), and DAPI (blue), and imaged using confocal microscopy. Regions selected for magnification are indicated by dotted white boxes. Bar, 5 μ m. (B) The percentage of σ NS immunofluorescence signal in reovirus factory-like structures was quantified by dividing the sum of σ NS signal in reovirus factory-like structures by the sum of cytoplasmic σ NS signal. Individual data points represent single cells. Percentage values that differ significantly from those obtained from WT σ NS and μ NS cotransfected cells by one-way analysis of variance (ANOVA) with Dunnett’s multiple-comparison test are shown. ****, $P < 0.0001$.

maintained a predominantly factory distribution. These results suggest that as viral factories mature, some viral mRNAs distribute to different intracellular sites.

WT σ NS and μ NS are sufficient to recruit viral mRNA to factory-like structures.

The lack of viral mRNAs in factories formed in the presence of mutant σ NS could be independent of viral mRNA incorporation into viral factories and instead due to impaired viral replication, leading to reduced secondary rounds of viral transcription. To uncouple viral mRNA distribution from viral replication, we transfected HEK293T cells with

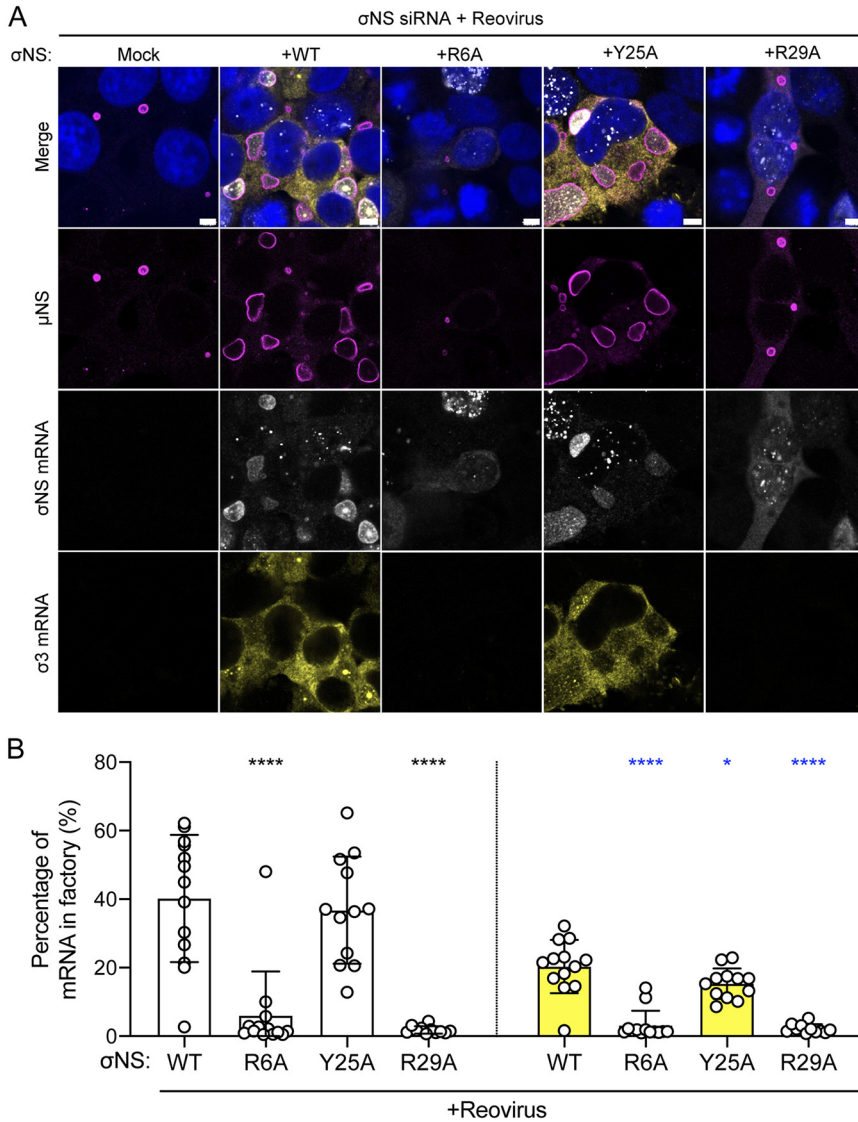


FIG 6 Reovirus transcripts are present in viral factories only when σ NS is capable of binding RNA. Cells that constitutively express siRNAs directed against σ NS were transfected with expression plasmids encoding the σ NS constructs shown and incubated for 24 h. Cells were adsorbed with reovirus strain T3D at an MOI of 5 PFU/cell, incubated for 48 h, fixed, stained using RNA FISH probes specific for σ NS mRNA (white) or σ 3 mRNA (yellow), μ NS-specific antiserum (magenta), and DAPI (blue), and imaged using confocal microscopy. Bar, 4.8 μ m. The percentage of cytoplasmic σ NS-mRNA (B, white bars) and σ 3-mRNA (B, yellow bars) FISH signals in reovirus factories was quantified by dividing the sum of the FISH signal in reovirus factories by the sum of the cytoplasmic FISH signal. Individual data points represent single cells. Percentage values that differ significantly from those obtained from WT σ NS-transfected reovirus-infected cells by one-way analysis of variance (ANOVA) with Dunnett's multiple-comparison test are shown. *, $P < 0.0332$; ****, $P < 0.0001$.

different combinations of expression plasmids encoding μ NS, WT or mutant forms of σ NS, and σ 3, fixed and stained them for FISH, and imaged the cells using confocal immunofluorescence microscopy (Fig. 7A). The σ 3 protein binds double-stranded RNA but not single-stranded RNA (24) and, thus, would not be expected to retain viral mRNA in factory-like structures. Concordantly, expression of μ NS and σ 3 was insufficient to promote incorporation of σ 3 mRNAs into factory-like structures (Fig. 7B, yellow). However, expression of μ NS and σ 3 along with WT or Y25A σ NS led to concentration of σ 3 mRNAs (Fig. 7B, yellow) as well as σ NS mRNAs in these structures (Fig. 7B, white). Neither σ NS nor σ 3 mRNAs concentrated in factory-like structures following expression of the R6A or R29A σ NS mutants with μ NS and σ 3. Instead, viral

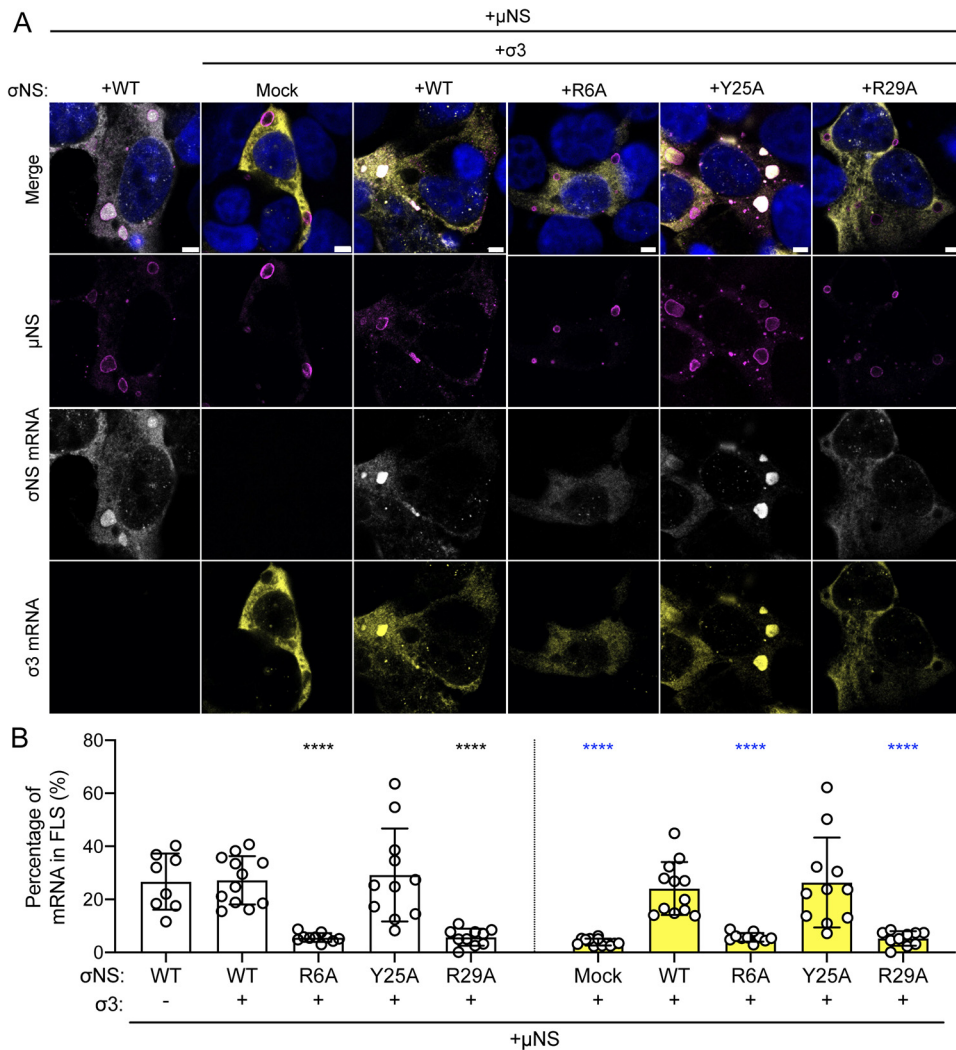


FIG 7 Reovirus mRNAs are recruited to factory-like structures by σ NS. Cells were transfected with expression plasmids encoding μ NS, σ 3, and the σ NS constructs shown and incubated for 24 h. Cells were fixed, stained using RNA FISH probes specific for σ NS mRNA (white) or σ 3 mRNA (yellow), μ NS-specific antiserum (magenta), and DAPI (blue), and imaged using confocal microscopy. Bar, 4.8 μ m. The percentage of cytoplasmic σ NS-mRNA (B, white bars) and σ 3-mRNA (B, yellow bars) FISH signals in factory-like structures was quantified by dividing the sum of the FISH signal in factory-like structures by the sum of the cytoplasmic FISH signal. Individual data points represent single cells. Percentage values that differ significantly from those obtained from cells cotransfected with WT σ NS, σ 3, and μ NS by one-way analysis of variance (ANOVA) with Dunnett's multiple-comparison test are shown. ****, $P < 0.0001$.

mRNAs appeared to be excluded from the interior of factory-like structures in the presence of these mutant σ NS proteins. Since the plasmids are transcribed in the nucleus, these data suggest that σ NS functions to recruit viral mRNAs into cytoplasmic factory-like structures. Collectively, these results suggest that σ NS is required to recruit viral mRNAs to reovirus factories.

DISCUSSION

In this study, we discovered a function for σ NS in reovirus factory formation. We found that σ NS requires electrostatic interactions to bind RNA and that RNA is not required to facilitate σ NS- μ NS interactions. We also observed that impeding σ NS-RNA binding disrupts viral mRNA incorporation into viral factory scaffolds. Reovirus factories that form in the presence of σ NS mutants incapable of binding RNA do not produce

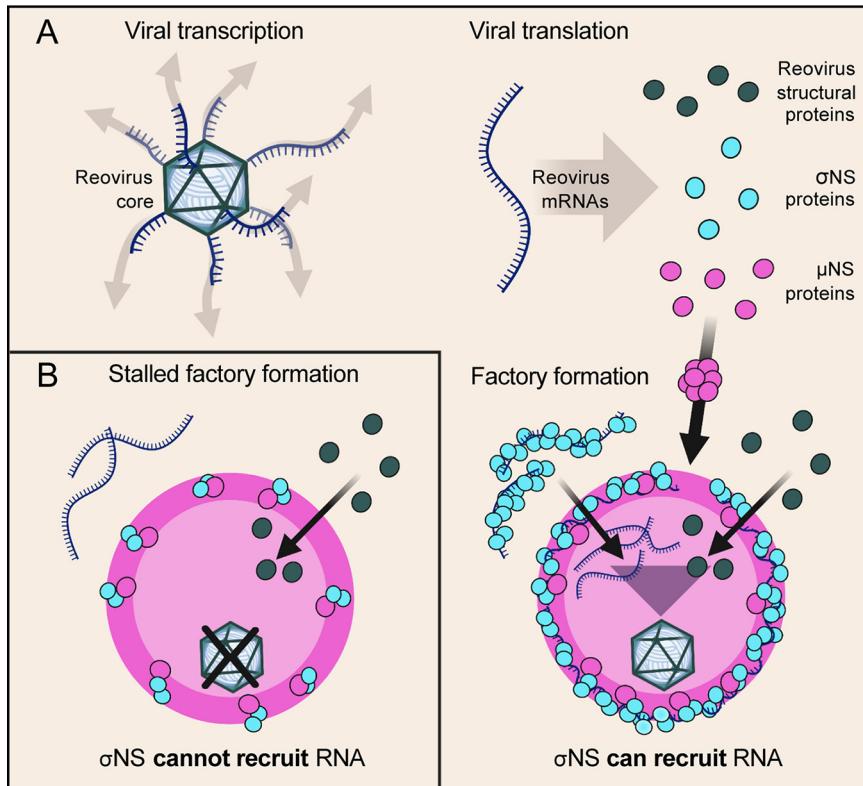


FIG 8 Model of σ NS mRNA recruitment for reovirus factory formation. (A) Following viral attachment and internalization, reovirus cores enter the cytoplasm and transcribe viral mRNAs that are translated to yield structural and nonstructural (NS) proteins. Factory scaffolds are formed by μ NS (large magenta sphere), which recruits reovirus structural proteins. Viral mRNAs in the cytoplasm are bound by σ NS and delivered to factory scaffolds. Viral components that form nascent viral cores are concentrated in factories, promoting viral packaging and core maturation for secondary rounds of transcription and translation. (B) Mutations in σ NS that compromise RNA-binding capacity also impede recruitment of mRNAs to factories and stall factory enlargement, as nascent cores do not form and are thus incapable of amplifying viral replication. This figure was prepared using BioRender.

progeny viral particles. A model of σ NS recruiting viral mRNAs for reovirus factory formation is shown in Fig. 8.

The manner in which RNA-binding proteins interact with RNA can influence the biological function of the resulting ribonucleoprotein complexes. Our data suggest that electrostatic interactions are required for reovirus σ NS to bind RNA (Fig. 2). These interactions could occur between an RNA base or the RNA phosphate backbone and positively charged residues in the N-terminal region of σ NS. Similarly, avian reovirus σ NS also requires positively charged residues in its N terminus (R6 and R11) to bind ssRNAs *in vitro* (25). Avian reovirus σ NS additionally displays RNA chaperone activity *in vitro* (26), suggesting another potential function for σ NS is to fold viral mRNAs. Certain mRNA structures could enhance RNA-RNA interactions between different viral mRNA segments, allowing precise packaging of 10 unique viral mRNAs into progeny viral particles (4). Rotavirus NSP2, which has been hypothesized to be a functional homolog of σ NS (26), also binds RNA using electrostatic interactions and, analogous to avian reovirus σ NS, chaperones rotavirus mRNAs (25). NSP2 regulates RNA-binding using residues that electrostatically repulse RNA (27). While we have identified residues required for σ NS to bind RNA, questions about the regulation and specificity of RNA binding remain. σ NS may displace RNA similarly to NSP2 or by some type of posttranslational modification (28). Aside from cellular contexts, σ NS does not preferentially bind viral mRNAs (16). However, in the context of viral infection, we hypothesize that σ NS preferentially binds and concentrates viral mRNAs in factories. Concentrating host mRNAs in viral factories may compromise viral packaging, as viral mRNAs would have to compete

with cellular mRNAs for RNA-RNA interactions. In support of this idea, RNA-binding specificity of other RNA-binding proteins differs *in vitro* and in cells (29). Future studies of σ NS-RNA binding could help fill these knowledge gaps and explain how σ NS controls the selective uptake of viral mRNAs into reovirus factories. Such a mechanism of control could be exploited to modulate the types of RNAs recruited into factory-like structures (30).

The charge-to-alanine mutations in the N terminus of σ NS engineered in this study do not impair interactions of σ NS with μ NS as detected by co-immunoprecipitation (Fig. 1D). However, mutant forms of σ NS incapable of RNA binding are not recruited to factories (Fig. 4A) or factory-like structures nucleated by μ NS (Fig. 5A). There are three possible explanations for the inconsistency of our co-immunoprecipitation and colocalization results. First, since the same general N-terminal region of σ NS (residues 1 to 11) is required for binding to RNA and μ NS (13, 31), mutations that disrupt RNA binding may allow enhanced accessibility of that region to interact with μ NS. Second, σ NS could bind μ NS proteins that have not integrated into the factory scaffolds. Third, σ NS could bind μ NS more avidly during cell lysis. The process of cell lysis likely disrupts the stability of factories and factory-like structures, which would allow increased access of σ NS to μ NS compared to that expected in viral factories.

Reovirus σ NS is required for a step or steps in viral replication at or prior to dsRNA synthesis by the viral polymerase (19). Based on previous results, σ NS interactions with viral mRNAs could enhance the stability of mRNAs bound at early stages of infection (19). However, based on our findings, we think that σ NS is also required for the formation of functional viral factories, which precedes dsRNA synthesis (32). The morphology of viral factories does not change dramatically in the absence of σ NS, but factories are notably smaller when σ NS is absent (19) (Fig. 4). During viral factory morphogenesis, σ NS likely alters factory scaffold properties to allow RNA incorporation. Viral mRNAs are thought to be packaged into nascent core particles in viral factories during assembly of reovirus progeny. σ NS mutants incapable of binding RNA retain the capacity to be recruited to factory structures, albeit to a lesser degree. However, σ NS distribution to factories is insufficient for its function in reovirus replication. σ NS additionally requires RNA-binding capacity, which mediates incorporation of viral mRNAs into factories. The accumulation of viral mRNAs (recruited by σ NS) and viral structural proteins (recruited by μ NS) within factories establishes an environment replete with viral components. Progeny virions then can form and amplify viral replication to yield much larger factories.

While our findings enhance an understanding of σ NS function during early steps in reovirus replication, questions remain about other potential functions of this protein. In addition to a potential role as an RNA chaperone, it is possible that σ NS enhances interactions between the viral polymerase and mRNAs, as observed for other viral RNA-binding proteins (33–37). Any of these observed or potential functions require that σ NS dissociate from viral mRNAs, as σ NS is not contained in mature viral particles (38). The mechanism underlying mRNA release from σ NS is not known, and it is not apparent at precisely what site in the cell such dissociation would occur. As factories enlarge, σ NS concentrates at the factory periphery (23) (see Fig. S4 in the supplemental material), suggesting that σ NS dissociates from RNA at that site. However, it also is possible that σ NS dissociates from RNAs in the factory center, as the protein is detectable throughout factories, albeit in more limited quantities, especially in larger factories.

Formation of functional reovirus factories also requires cellular factors, many of which are unknown. Therefore, it is possible that σ NS modifies host components in some way to promote factory formation and viral replication. Expression of σ NS in the absence of other viral proteins induces endoplasmic reticulum (ER) tubulation (39). This morphological change is hypothesized to culminate in the formation of the ER fragments embedded in reovirus factories during infection. σ NS could facilitate the incorporation of ER fragments into factories by binding ER-resident RNAs or proteins or engaging ER lipids. While the function of the ER fragments within factories has not

been established, we think that the membranes provide a physical matrix to allow viral packaging, as observed for many RNA viruses (40). Proteins essential for the integrated stress response also are implicated in reovirus replication (41–43). In stressed cells, σ NS recruits G3BP1 and other stress granule proteins to factory-like structures (44). The recruitment of stress granule proteins to factories depends on RNA and could lead to recruitment of the translational machinery, usually found within stress granules, to viral factories (23). These activities could occur concomitantly with viral mRNA recruitment by σ NS.

Membrane enclosure is the most broadly known mechanism for organelles to compartmentalize intracellular components required for efficient molecular interactions and functions. However, organelles can form using a process of liquid-liquid phase separation (45). Liquid-liquid phase separation leads to the development of dynamic organelles, called condensates, that are stabilized by multivalent interactions between proteins, nucleic acids, or both (45). These organelles can separate from the intracellular environment, selectively package discrete constituents, and allow biochemical activities, such as viral genome replication and capsid assembly, to be coordinated with high efficiency (46). Many RNA viruses use this mechanism to form viral factories (47–51). While development of many types of liquid-liquid phase-separated condensates of both viral and cellular origin depends on RNA, the formation of reovirus factories may differ (52). Since reovirus mRNAs are excluded from the factory-like structures formed solely by μ NS, it is likely that μ NS does not require RNA to phase separate. In this way, reovirus factory-like structures resemble other condensates that do not require RNA to mediate multivalent interactions (53, 54). For example, the formation of measles virus factories also does not require RNA, and a viral RNA-binding protein, N protein, can recruit RNA to factory-like structures to efficiently form RNP complexes within (50). Future studies will identify the minimal constituents and conditions required to form reovirus factory condensates and define the biophysical changes that occur when other components are added.

Experiments reported here indicate that σ NS incorporates viral mRNAs into reovirus factory scaffolds that naturally exclude viral mRNAs. Our work begins to uncover how a dsRNA virus factory controls the selectivity of its composition. The next steps include defining the specificity of σ NS interactions with RNA and identifying additional molecular interactants that enable σ NS to promote viral genome replication and packaging. These studies are anticipated to illuminate new targets to impede dsRNA virus replication, which may have broad utility.

MATERIALS AND METHODS

Cells, viruses, and plasmids. HEK293T cells and HEK293T cells expressing a GFP-specific siRNA (GFP-siRNA cells) (19) or an S3-specific siRNA (σ NS-siRNA cells) (19) were maintained in Dulbecco's modified Eagle's medium (DMEM) supplemented to contain 5% fetal bovine serum (FBS) and 2 mM L-glutamine (Life Technologies). Culture medium for the siRNA-expressing cells was additionally supplemented to contain 5 μ g/ml of puromycin (InvivoGen). L929 (L) cells adapted for growth in spinner cultures were maintained in Joklik's minimal essential medium (JMEM) supplemented to contain 5% FBS, 1% L-glutamine, 50 U/ml of penicillin, 50 μ g/ml of streptomycin (Life Technologies), and 0.25 μ g/ml amphotericin B (Sigma). HeLa CCL2 cells were grown in DMEM supplemented to contain 10% FBS, 1% sodium pyruvate (Gibco), 1% MEM nonessential amino acids (Sigma-Aldrich), 1% L-glutamine, 50 U/ml of penicillin, 50 μ g/ml of streptomycin, and 0.25 μ g/ml amphotericin B.

WT reovirus strain T3D was recovered using reverse genetics (55). Site-directed mutagenesis of the reverse genetics plasmid encoding σ NS was used to engineer σ NS with R6A, K11A, and R29A mutations. Viruses encoding these mutations were not recovered using reverse genetics. Primers used for mutagenesis are listed in Table S1 in the supplemental material. Reovirus strain T1L M1-P208S (56) was recovered using reverse genetics (55). Reovirus T1L M1-P208S contains a point mutation in the M1 gene that causes viral factories to have a globular morphology similar to the morphology of factories formed by reovirus T3D (56). Viruses were amplified in L cells and purified by cesium chloride gradient centrifugation as described previously (57). Viral titers were determined by plaque assay using L cells (58).

Reovirus T3D σ 3 (59), WT σ NS (19), Δ 38 σ NS (19), and GFP (59) expression plasmids have been described elsewhere. T3D μ NS expression plasmid was engineered by amplification of the T3D M3 open reading frame to contain 5' KpnI and 3' NotI restriction sites using reverse-genetics plasmid pT7-M3T3D (60) and T3D M3 5'-KpnI-NotI-3' primers listed in Table S1. The amplified DNA was digested with NotI-HF and KpnI-HF (New England BioLabs [NEB]) and purified from agarose gel fragments following

electrophoresis. The purified PCR product was ligated into pcDNA3.1+ vectors between the NotI-HF and KpnI-HF restriction sites. Site-directed mutagenesis was used to engineer σ NS expression plasmids encoding R6A, K11A, R14A, TriA, Y25A, R29A, K35A, and R38A with primers listed in Table S1. Fidelity of cloning and mutagenesis was confirmed using Sanger sequencing (Genewiz) and Genewiz primers T7 and BGHR.

Expression, proteolysis, and RNA-dependent oligomerization assays. Reovirus σ NS proteins were expressed from plasmids *in vitro* using the TNT T7 polymerase-coupled rabbit-reticulocyte lysate system (Promega, L4610) (19). Reactions were supplemented with [³⁵S]methionine (Perkin Elmer, NEG709A500UC), incubated at 30°C for 1.5 h, and terminated with a 4-fold dilution in stop buffer (20 mM HEPES-KOH [pH 7.4], 100 mM potassium acetate, 5 mM magnesium acetate, 5 mM EDTA, 2 mM methionine, and freshly supplemented to contain 1 mM dithiothreitol [DTT] and 2 mM puromycin). Terminated reactions were used for proteolysis and RNA-dependent oligomerization assays.

Proteolysis assays were conducted by incubating translation reactions with 1 μ g/ml proteinase K (Sigma) at 37°C for 0, 5, 10, or 15 min. Samples were prepared for sodium dodecyl sulfate-polyacrylamide gel electrophoresis (SDS-PAGE).

RNA-dependent oligomerization assays were conducted by incubating translation reactions with 10 μ g of RNase A (Thermo Fisher) or 125 mM NaCl at 37°C for 1 h. Samples were prepared for native PAGE and SDS-PAGE.

Native PAGE, SDS-PAGE, phosphorimaging, and immunoblotting. Samples for native PAGE were diluted in 4 \times native PAGE sample buffer (Thermo Fisher) and electrophoresed in 4% to 16% native PAGE bis-Tris acrylamide gels (Thermo Fisher) using the Blue native PAGE Novex bis-Tris gel system (Thermo Fisher) at 4°C as described previously (19). Samples for denaturing SDS-PAGE were boiled in SDS-PAGE sample buffer (Bio-Rad) containing β -mercaptoethanol and electrophoresed in 4% to 20% Mini-Protean TGX gels (Bio-Rad).

Polyacrylamide gels containing ³⁵S-labeled proteins were fixed with 40% methanol and 10% acetic acid at room temperature (RT) for 30 min, washed with double-distilled water (ddH₂O), and dried onto filter paper using a gel dryer (Bio-Rad). Dried gels were exposed on a phosphorimaging screen and imaged using a phosphor system scanner (Perkin Elmer, B431200). Band intensities were quantified using ImageJ software.

Polyacrylamide gels containing unlabeled proteins were transferred to nitrocellulose membranes (Bio-Rad) and immunoblotted using the following antibodies: guinea pig σ NS-specific polyclonal antiserum (19), chicken μ NS-specific polyclonal antiserum (19), and mouse α -tubulin-specific monoclonal antibody (Cell Signaling Technology). IRDye 800CW donkey anti-guinea pig, IRDye 680RD donkey anti-chicken, and IRDye 680LT goat anti-mouse IgG antibodies (Li-Cor) were used as detection reagents. Antibodies were diluted at the following dilutions: 1:1,000 for guinea pig σ NS-specific antiserum, 1:5,000 for chicken μ NS-specific antiserum, 1:1,000 for mouse α -tubulin-specific antibody, and 1:7,500 for secondary antibodies. Immunoblot images were captured using an Odyssey CLx imaging system (Li-Cor).

Immunoprecipitation and co-immunoprecipitation assays. HEK293T cells were transfected with σ NS expression plasmids alone or in combination with μ NS expression plasmid using FuGene 6 transfection reagent (Promega) at a reagent/DNA ratio of 3:1 in Opti-MEM (Life Technologies). At 24 h post-transfection, cells were lysed with IP lysis buffer (25 mM Tris [pH 7.4], 150 mM NaCl, 1% NP-40 substitute [VWR], 0.5% deoxycholate [DOC], 0.1% SDS) on ice for 30 min or co-IP buffer (20 mM Tris [pH 7.5], 137 mM NaCl, 2 mM EDTA, 0.1% NP-40 substitute) at 4°C for 30 min with rotation. Lysis buffers were supplemented with protease inhibitors (Roche, 11873580001) before use. Following lysis, cellular debris was collected by centrifugation at 20,000 \times g at 4°C for 20 min. Supernatants were incubated with protein G Dynabeads (Thermo Fisher, 10004D) saturated with σ NS-specific monoclonal 2A9 (IP [10]) or 3E10 (co-IP [10]) antibodies at 4°C for 4 h with rotation. Antibodies were saturated on Dynabeads according to the manufacturer's protocol. Dynabeads were washed with cold lysis buffer, and bound proteins were eluted by boiling in SDS-PAGE sample buffer (Bio-Rad) with β -mercaptoethanol for 10 min. Proteins were analyzed by immunoblotting.

σ NS complementation assays. GFP or σ NS siRNA-expressing cells were cultivated in 6-well plates for virus quantification or 8-well cell culture slides for immunofluorescence (Ibidi, 80826; fluorescence *in situ* hybridization: MatTek, CCS-8). Cells were transfected with GFP or σ NS expression plasmids using FuGene 6 transfection reagent. At 24 h posttransfection, cells were adsorbed with reovirus at a multiplicity of infection (MOI) of 5 PFU/cell. Following incubation at 37°C for 48 h, the supernatant was collected, and viral titers were determined by plaque assay. Cells cultivated on slides were processed for fluorescence microscopy.

Immunogold labeling of Tokuyasu cryosections. HeLa cells were adsorbed with reovirus T1L M1-P208S at an MOI of 1 PFU/cell. Following incubation at 37°C for 14 h, cells were fixed with 4% paraformaldehyde (PFA) in 0.2 M HEPES buffer (pH 7.4) at RT for 2 h. Free aldehyde groups were quenched with 50 mM NH₄Cl. Cells were removed from the plates with a rubber policeman and pelleted by centrifugation in a 1.5-ml Eppendorf tube. The cell pellet was embedded in 12% gelatin (TAAB Laboratories) in phosphate-buffered saline (PBS), and after solidification, cubes of 1 mm³ were cut and infiltrated with 2.3 M sucrose in PBS at 4°C overnight. Cubes were mounted on metal pins and frozen in liquid nitrogen. Thin cryosections were obtained at -120°C using an FC6 cryo-ultramicrotome (Leica Microsystems), collected from the diamond knife into a 1:1 mixture of 2% methylcellulose in H₂O and 2.3 M sucrose in PBS, and placed after thawing on 200-mesh grids with a carbon-coated Formvar film. Grids were incubated with σ NS-specific monoclonal antibody 2F5 (10) diluted 1:200 in saturation buffer (1% bovine serum albumin [BSA] in PBS) at RT for 1 h. Secondary antibody conjugated with 10-nm colloidal gold particles

(British Biocell Int.) was diluted 1:50 in saturation buffer, and grids were incubated at RT for 30 min. After labeling, images were captured using a JEOL JEM-1011 transmission electron microscope operating at 100 kV. At least two independent labeling assays were conducted for each experimental condition.

Factory-like structure assays. HEK293T σ NS siRNA-expressing cells or HEK293T cells were cultivated in 8-well cell culture slides (immunofluorescence, Ibdid; fluorescence *in situ* hybridization, MatTek). Cells were transfected with various combinations of σ 3, σ NS, and μ NS expression plasmids using FuGene 6 transfection reagent. For combinations of fewer than three plasmids, empty pcDNA3.1+ plasmid was added to the transfection mixtures to maintain identical DNA concentrations for all conditions. At 24 to 48 h posttransfection, cells were processed for fluorescence microscopy.

Immunofluorescence assays. Cells were fixed with 4% paraformaldehyde (PFA) diluted in PBS at RT for 30 min, permeabilized in 1% Triton X-100 in PBS at RT for 10 min, and blocked with PBS containing 0.5% bovine serum albumin, 0.1% glycine, 0.05% Tween 20 (PBS-BGT) at 37°C for 10 min. Cells were incubated with σ NS-specific monoclonal antibody 3E10 and chicken μ NS-specific polyclonal antiserum diluted in PBS-BGT at RT for 1 h, washed with PBS-BGT, probed with species-specific secondary antibodies conjugated with Alexa Fluor 488 or 647 (Thermo Fisher), and counterstained with 4',6-diamidino-2-phenylindole (DAPI; Invitrogen) to label nuclei. Cells were washed with PBS-BGT and stored in PBS. Antibodies were diluted 1:1,000 for antibody 3E10, 1:1,000 for μ NS-specific antiserum, and 1:1,000 for secondary antibodies.

Cell images were captured using a Leica SP8 laser scanning confocal microscope equipped with a 63 \times oil lens objective. Images were processed and analyzed using ImageJ software with the Fiji processing package. The brightness of each channel was adjusted to that of the appropriate mock signals and normalized for all experimental conditions. The percentage of σ NS immunofluorescence signal intensities in factories and factory-like structures was calculated by marking high-intensity μ NS immunofluorescence as regions of interest (ROIs). Total σ NS immunofluorescence signal intensities within all ROIs of a single cell were determined and then divided by the total σ NS immunofluorescence signal intensities detected within the cytoplasm.

Fluorescence *in situ* hybridization microscopy. Cells were fixed with 3% PFA diluted in PBS for 30 min and permeabilized in 70% ethanol (EtOH) at 4°C overnight. Cells were rehydrated with wash buffer (10% formamide and 2 \times SSC [1 \times SSC is 0.15 M NaCl plus 0.015 M sodium citrate] in diethyl pyrocarbonate [DEPC]-treated water) and incubated with hybridization buffer (10% dextran sulfate, 2 mM vanadyl-ribonucleoside complex [NEB], 0.02% UltraPure BSA [Thermo Fisher], 1 mg/ml *Escherichia coli* tRNA [Sigma], 2 \times SSC, and 10% formamide in DEPC-treated water) containing a 1:1,000 dilution of chicken μ NS-specific antiserum and 100 nM σ NS (quasar670) or σ 3 (quasar570) mRNA FISH probes (Biosearch Technologies) at 28°C overnight. The mRNA FISH probe sets consisted of at least 20 probes of ~20 base pairs in length, and individual probes were designed to bind target sequences at a minimum spacing of two nucleotides between probes (Biosearch Technologies). Following hybridization, cells were washed with wash buffer and incubated with anti-chicken Alexa Fluor 488-conjugated antibody (Thermo Fisher) diluted to 1:1,000 in secondary buffer (2 mM vanadyl-ribonucleoside complex, 0.02% RNA-free BSA, 1 mg/ml *E. coli* tRNA, 2 \times SSC, and 10% formamide in DEPC-treated water) at RT for 1 h. Cells were washed with wash buffer and counterstained with DAPI. Glass coverslips were mounted on labeled cells using Prolong Diamond antifade mounting medium (Thermo Fisher).

Cell images were captured using a Leica SP8 laser scanning confocal microscope equipped with a 63 \times oil lens objective. Images were processed and analyzed using ImageJ software with the Fiji processing package. The brightness of each channel was adjusted to that of the appropriate mock signals and normalized for all experimental conditions. The percentage of FISH signal intensities in factories and factory-like structures was calculated by marking high-intensity μ NS immunofluorescence as ROIs. Total FISH signal intensities within all the ROIs of a cell were determined and then divided by the total FISH signal intensities detected within the cytoplasm.

Statistical analysis. All experiments were conducted with two to three biological replicates. Data are presented as the mean \pm standard error of the mean unless otherwise indicated. Ordinary one-way analyses of variance (ANOVAs) were conducted with Dunnett's multiple-comparison test. All data and statistical analyses were conducted using GraphPad Prism 8 data analysis software.

SUPPLEMENTAL MATERIAL

Supplemental material is available online only.

FIG S1, PDF file, 0.1 MB.

FIG S2, PDF file, 0.1 MB.

FIG S3, PDF file, 0.2 MB.

FIG S4, PDF file, 0.2 MB.

FIG S5, PDF file, 0.2 MB.

TABLE S1, PDF file, 0.1 MB.

ACKNOWLEDGMENTS

We thank Anthony Lentscher, Pengcheng Shang, and Danica Sutherland for review of the manuscript and members of the Dermody laboratory for many useful discussions. We

also thank the UPMC Children's Hospital of Pittsburgh Rangos Research Center Cell Imaging Core Laboratory for assistance with microscopy.

This work was supported by Public Health Service awards R01 AI121216 (J.S.L.P.) and R01 AI032539 (C.R. and T.S.D.), UPMC Children's Hospital of Pittsburgh (K.R.), and the Heinz Endowments (T.S.D.).

REFERENCES

- Fernández de Castro I, Tenorio R, Risco C. 2020. Virus factories, p 495–500. In Bamford DJ, Zuckerman M (ed), *Encyclopedia of virology*, 4th ed. Academic Press, Cambridge, MA. <https://doi.org/10.1016/B978-0-12-814515-9.00001-1>.
- Bouziat R, Hinterleitner R, Brown JJ, Stencel-Baerenwald JE, Iklizler M, Mayassi T, Meisel M, Kim SM, Discepolo V, Pruijssers AJ, Ernest JD, Iskarpatyoti JA, Costes LM, Lawrence I, Palanski BA, Varma M, Zurenski MA, Khomandiak S, McAllister N, Aravamudhan P, Boehme KW, Hu F, Samsom JN, Reinecker HC, Kupfer SS, Guandalini S, Semrad CE, Abadie V, Khosla C, Barreiro LB, Xavier RJ, Ng A, Dermody TS, Jabri B. 2017. Reovirus infection triggers inflammatory responses to dietary antigens and development of celiac disease. *Science* 356:44–50. <https://doi.org/10.1126/science.aah5298>.
- Phillips MB, Stuart JD, Rodriguez Stewart RM, Berry JT, Mainou BA, Boehme KW. 2018. Current understanding of reovirus oncolysis mechanisms. *Oncolytic Virother* 7:53–63. <https://doi.org/10.2147/OV.S143808>.
- Borodavka A, Desselberger U, Patton JT. 2018. Genome packaging in multi-segmented dsRNA viruses: distinct mechanisms with similar outcomes. *Curr Opin Virol* 33:106–112. <https://doi.org/10.1016/j.coviro.2018.08.001>.
- Danthi P, Guglielmi KM, Kirchner E, Mainou B, Stehle T, Dermody TS. 2010. From touchdown to transcription: the reovirus cell entry pathway. *Curr Top Microbiol Immunol* 343:91–119. https://doi.org/10.1007/82_2010_32.
- Eichwald C, Ackermann M, Nibert ML. 2018. The dynamics of both filamentous and globular mammalian reovirus viral factories rely on the microtubule network. *Virology* 518:77–86. <https://doi.org/10.1016/j.virol.2018.02.009>.
- Bussiere LD, Choudhury P, Bellaire B, Miller CL. 2017. Characterization of a replicating mammalian orthoreovirus with tetracysteine-tagged μ NS for live-cell visualization of viral factories. *J Virol* 91:e01371-17. <https://doi.org/10.1128/JVI.01371-17>.
- Fernandez de Castro I, Zamora PF, Ooms L, Fernandez JJ, Lai CM, Mainou BA, Dermody TS, Risco C. 2014. Reovirus forms neo-organelles for progeny particle assembly within reorganized cell membranes. *mBio* 5:e00931-13. <https://doi.org/10.1128/mBio.00931-13>.
- Becker MM, Peters TR, Dermody TS. 2003. Reovirus σ NS and μ NS proteins form cytoplasmic inclusion structures in the absence of viral infection. *J Virol* 77:5948–5963. <https://doi.org/10.1128/JVI.77.10.5948-5963.2003>.
- Becker MM, Goral MI, Hazelton PR, Baer GS, Rodgers SE, Brown EG, Coombs KM, Dermody TS. 2001. Reovirus σ NS protein is required for nucleation of viral assembly complexes and formation of viral inclusions. *J Virol* 75:1459–1475. <https://doi.org/10.1128/JVI.75.3.1459-1475.2001>.
- Broering TJ, Parker JS, Joyce PL, Kim J, Nibert ML. 2002. Mammalian reovirus nonstructural protein μ NS forms large inclusions and colocalizes with reovirus microtubule-associated protein μ 2 in transfected cells. *J Virol* 76:8285–8297. <https://doi.org/10.1128/jvi.76.16.8285-8297.2002>.
- Mudogo CN, Falke S, Brognaro H, Duzenko M, Betzel C. 2020. Protein phase separation and determinants of in cell crystallization. *Traffic* 21:220–230. <https://doi.org/10.1111/tra.12711>.
- Miller CL, Arnold MM, Broering TJ, Hastings CE, Nibert ML. 2010. Localization of mammalian orthoreovirus proteins to cytoplasmic factory-like structures via nonoverlapping regions of μ NS. *J Virol* 84:867–882. <https://doi.org/10.1128/JVI.01571-09>.
- Broering TJ, Kim J, Miller CL, Piggott CD, Dinoso JB, Nibert ML, Parker JS. 2004. Reovirus nonstructural protein mNS recruits viral core surface proteins and entering core particles to factory-like inclusions. *J Virol* 78:1882–1892. <https://doi.org/10.1128/jvi.78.4.1882-1892.2004>.
- Miller CL, Broering TJ, Parker JS, Arnold MM, Nibert ML. 2003. Reovirus σ NS protein localizes to inclusions through an association requiring the μ NS amino terminus. *J Virol* 77:4566–4576. <https://doi.org/10.1128/JVI.77.8.4566-4576.2003>.
- Gillian AL, Schmechel SC, Livny J, Schiff LA, Nibert ML. 2000. Reovirus protein σ NS binds in multiple copies to single-stranded RNA and shares properties with single-stranded DNA binding proteins. *J Virol* 74:5939–5948. <https://doi.org/10.1128/jvi.74.13.5939-5948.2000>.
- Antczak JB, Joklik WK. 1992. Reovirus genome segment assortment into progeny genomes studied by the use of monoclonal-antibodies directed against reovirus proteins. *Virology* 187:760–776. [https://doi.org/10.1016/0042-6822\(92\)90478-8](https://doi.org/10.1016/0042-6822(92)90478-8).
- Stamatos NM, Gomatos PJ. 1982. Binding to selected regions of reovirus mRNAs by a nonstructural reovirus protein. *Proc Natl Acad Sci U S A* 79:3457–3461. <https://doi.org/10.1073/pnas.79.11.3457>.
- Zamora PF, Hu L, Knowlton JJ, Lahr RM, Moreno RA, Berman AJ, Prasad BVV, Dermody TS. 2018. Reovirus nonstructural protein σ NS acts as an RNA-stability factor promoting viral genome replication. *J Virol* 92:e00563-18. <https://doi.org/10.1128/JVI.00563-18>.
- Goral MI, Mochow-Grundy M, Dermody TS. 1996. Sequence diversity within the reovirus S3 gene: reoviruses evolve independently of host species, geographic locale, and date of isolation. *Virology* 216:265–271. <https://doi.org/10.1006/viro.1996.0059>.
- Corley M, Burns MC, Yeo GW. 2020. How RNA-binding proteins interact with RNA: molecules and mechanisms. *Mol Cell* 78:9–29. <https://doi.org/10.1016/j.molcel.2020.03.011>.
- Parker JS, Broering TJ, Kim J, Higgins DE, Nibert ML. 2002. Reovirus core protein μ 2 determines the filamentous morphology of viral inclusion bodies by interacting with and stabilizing microtubules. *J Virol* 76:4483–4496. <https://doi.org/10.1128/jvi.76.9.4483-4496.2002>.
- Desmet EA, Anguish LJ, Parker JS. 2014. Virus-mediated compartmentalization of the host translational machinery. *mBio* 5:e01463-14–e01414. <https://doi.org/10.1128/mBio.01463-14>.
- Huismans H, Joklik WK. 1976. Reovirus-coded polypeptides in infected cells: isolation of two native monomeric polypeptides with high affinity for single-stranded and double-stranded RNA, respectively. *Virology* 70:411–424. [https://doi.org/10.1016/0042-6822\(76\)90282-8](https://doi.org/10.1016/0042-6822(76)90282-8).
- Touris-Otero F, Martinez-Costas J, Vakharia VN, Benavente J. 2005. Characterization of the nucleic acid-binding activity of the avian reovirus non-structural protein σ NS. *J Gen Virol* 86:1159–1169. <https://doi.org/10.1099/vir.0.80491-0>.
- Borodavka A, Ault J, Stockley PG, Tuma R. 2015. Evidence that avian reovirus σ NS is an RNA chaperone: implications for genome segment assortment. *Nucleic Acids Res* 43:7044–7057. <https://doi.org/10.1093/nar/gkv639>.
- Bravo JPK, Bartnik K, Venditti L, Gail EH, Davidovich C, Lamb DC, Tuma R, Calabrese AN, Borodavka A. 5 January 2020. Structural basis of rotavirus RNA chaperone displacement and RNA annealing. *bioRxiv* <https://doi.org/10.1101/2020.10.26.354233>.
- Lovci MT, Bengtson MH, Massirer KB. 2016. Post-translational modifications and RNA-binding proteins. *Adv Exp Med Biol* 907:297–317. https://doi.org/10.1007/978-3-319-29073-7_12.
- Jankowsky E, Harris ME. 2015. Specificity and nonspecificity in RNA-protein interactions. *Nat Rev Mol Cell Biol* 16:533–544. <https://doi.org/10.1038/nrm4032>.
- García-Jove Navarro M, Kashida S, Chouaib R, Souquere S, Pierron G, Weill D, Gueroui Z. 2019. RNA is a critical element for the sizing and the composition of phase-separated RNA-protein condensates. *Nat Commun* 10:3230. <https://doi.org/10.1038/s41467-019-11241-6>.
- Gillian AL, Nibert ML. 1998. Amino terminus of reovirus nonstructural protein σ NS is important for ssRNA binding and nucleoprotein complex formation. *Virology* 240:1–11. <https://doi.org/10.1006/viro.1997.8905>.
- Tenorio R, Fernández de Castro I, Knowlton JJ, Zamora PF, Sutherland DM, Risco C, Dermody TS. 2019. Function, architecture, and biogenesis of reovirus replication neorganelles. *Viruses* 11:288. <https://doi.org/10.3390/v11030288>.
- Stork J, Kovalev N, Sasvari Z, Nagy PD. 2011. RNA chaperone activity of the tombusviral p33 replication protein facilitates initiation of RNA synthesis by the viral RdRp *in vitro*. *Virology* 409:338–347. <https://doi.org/10.1016/j.virol.2010.10.015>.
- Arnoldi F, Campagna M, Eichwald C, Desselberger U, Burrone OR. 2007. Interaction of rotavirus polymerase VP1 with nonstructural protein NSP5 is stronger than that with NSP2. *J Virol* 81:2128–2137. <https://doi.org/10.1128/JVI.01494-06>.

35. Mir MA, Panganiban AT. 2006. The bunyavirus nucleocapsid protein is an RNA chaperone: possible roles in viral RNA panhandle formation and genome replication. *RNA* 12:272–282. <https://doi.org/10.1261/rna.2101906>.
36. Mir MA, Panganiban AT. 2006. Characterization of the RNA chaperone activity of hantavirus nucleocapsid protein. *J Virol* 80:6276–6285. <https://doi.org/10.1128/JVI.00147-06>.
37. Ruigrok RW, Crépin T. 2010. Nucleoproteins of negative strand RNA viruses; RNA binding, oligomerisation and binding to polymerase co-factor. *Viruses* 2:27–32. <https://doi.org/10.3390/v2010027>.
38. Smith RE, Zweerink HJ, Joklik WK. 1969. Polypeptide components of virions, top component and cores of reovirus type 3. *Virology* 39:791–810. [https://doi.org/10.1016/0042-6822\(69\)90017-8](https://doi.org/10.1016/0042-6822(69)90017-8).
39. Tenorio R, Fernández de Castro I, Knowlton JJ, Zamora PF, Lee CH, Mainou BA, Dermody TS, Risco C. 2018. Reovirus σ NS and μ NS proteins remodel the endoplasmic reticulum to build replication neorganelles. *mBio* 9:e01253-18. <https://doi.org/10.1128/mBio.01253-18>.
40. Fernández de Castro I, Tenorio R, Risco C. 2016. Virus assembly factories in a lipid world. *Curr Opin Virol* 18:20–26. <https://doi.org/10.1016/j.coviro.2016.02.009>.
41. Qin Q, Hastings C, Miller CL. 2009. Mammalian orthoreovirus particles induce and are recruited into stress granules at early times postinfection. *J Virol* 83:11090–11101. <https://doi.org/10.1128/JVI.01239-09>.
42. Smith JA, Schmechel SC, Raghavan A, Abelson M, Reilly C, Katze MG, Kaufman RJ, Bohjanen PR, Schiff LA. 2006. Reovirus induces and benefits from an integrated cellular stress response. *J Virol* 80:2019–2033. <https://doi.org/10.1128/JVI.80.4.2019-2033.2006>.
43. Lutz MMt, Worth MP, Hinchman MM, Parker JSL, Ledgerwood ED. 2019. Mammalian orthoreovirus infection is enhanced in cells pre-treated with sodium arsenite. *Viruses* 11:563. <https://doi.org/10.3390/v11060563>.
44. Choudhury P, Bussiere L, Miller CL. 2017. *Mammalian orthoreovirus* factories modulate stress granule protein localization by interaction with G3BP1. *J Virol* 91:e01298-17. <https://doi.org/10.1128/JVI.01298-17>.
45. Boeynaems S, Alberti S, Fawzi NL, Mittag T, Polymenidou M, Rousseau F, Schymkowitz J, Shorter J, Wolozin B, Van Den Bosch L, Tompa P, Fuxreiter M. 2018. Protein phase separation: a new phase in cell biology. *Trends Cell Biol* 28:420–435. <https://doi.org/10.1016/j.tcb.2018.02.004>.
46. Nakashima KK, Vibhute MA, Spruijt E. 2019. Biomolecular chemistry in liquid phase separated compartments. *Front Mol Biosci* 6:21. <https://doi.org/10.3389/fmolb.2019.00021>.
47. Nikolic J, Le Bars R, Lama Z, Scrima N, Lagaudrière-Gesbert C, Gaudin Y, Blondel D. 2017. Negri bodies are viral factories with properties of liquid organelles. *Nat Commun* 8:58. <https://doi.org/10.1038/s41467-017-00102-9>.
48. Heinrich BS, Maliga Z, Stein DA, Hyman AA, Whelan SPJ. 2018. Phase transitions drive the formation of vesicular stomatitis virus replication compartments. *mBio* 9:e02290-17. <https://doi.org/10.1128/mBio.02290-17>.
49. Galloux M, Risso-Ballester J, Richard CA, Fix J, Rameix-Welti MA, Eléouët JF. 2020. Minimal elements required for the formation of respiratory syncytial virus cytoplasmic inclusion bodies *in vivo* and *in vitro*. *mBio* 11:e01202-20. <https://doi.org/10.1128/mBio.01202-20>.
50. Guseva S, Milles S, Jensen MR, Salvi N, Kleman JP, Maurin D, Ruigrok RWH, Blackledge M. 2020. Measles virus nucleocapsid and phosphoproteins form liquid-like phase-separated compartments that promote nucleocapsid assembly. *Sci Adv* 6:eaaz7095. <https://doi.org/10.1126/sciadv.aaz7095>.
51. Nevers Q, Albertini AA, Lagaudrière-Gesbert C, Gaudin Y. 2020. Negri bodies and other virus membrane-less replication compartments. *Biochim Biophys Acta Mol Cell Res* 1867:118831. <https://doi.org/10.1016/j.bbamcr.2020.118831>.
52. Fay MM, Anderson PJ. 2018. The role of RNA in biological phase separations. *J Mol Biol* 430:4685–4701. <https://doi.org/10.1016/j.jmb.2018.05.003>.
53. Bracha D, Walls MT, Wei MT, Zhu L, Kurian M, Avalos JL, Toettcher JE, Brangwynne CP. 2018. Mapping local and global liquid phase behavior in living cells using photo-oligomerizable seeds. *Cell* 175:1467.e13–1480.e13. <https://doi.org/10.1016/j.cell.2018.10.048>.
54. Li P, Banjade S, Cheng HC, Kim S, Chen B, Guo L, Llaguno M, Hollingsworth JV, King DS, Banani SF, Russo PS, Jiang QX, Nixon BT, Rosen MK. 2012. Phase transitions in the assembly of multivalent signalling proteins. *Nature* 483:336–340. <https://doi.org/10.1038/nature10879>.
55. Kobayashi T, Ooms LS, Ikizler M, Chappell JD, Dermody TS. 2010. An improved reverse genetics system for mammalian orthoreoviruses. *Virology* 398:194–200. <https://doi.org/10.1016/j.virol.2009.11.037>.
56. Fernández de Castro I, Tenorio R, Ortega-González P, Knowlton JJ, Zamora PF, Lee CH, Fernández JJ, Dermody TS, Risco C. 2020. A modified lysosomal organelle mediates nonlytic egress of reovirus. *J Cell Biol* 219:e201910131. <https://doi.org/10.1083/jcb.201910131>.
57. Furlong DB, Nibert ML, Fields BN. 1988. Sigma 1 protein of mammalian reoviruses extends from the surfaces of viral particles. *J Virol* 62:246–256. <https://doi.org/10.1128/JVI.62.1.246-256.1988>.
58. Virgin HW, Bassel-Duby R, Fields BN, Tyler KL. 1988. Antibody protects against lethal infection with the neurally spreading reovirus type 3 (Dearing). *J Virol* 62:4594–4604. <https://doi.org/10.1128/JVI.62.12.4594-4604.1988>.
59. Knowlton JJ, Fernandez de Castro I, Ashbrook AW, Gestaut DR, Zamora PF, Bauer JA, Forrest JC, Frydman J, Risco C, Dermody TS. 2018. The TRiC chaperonin controls reovirus replication through outer-capsid folding. *Nat Microbiol* 3:481–493. <https://doi.org/10.1038/s41564-018-0122-x>.
60. Kobayashi T, Antar AA, Boehme KW, Danthi P, Eby EA, Guglielmi KM, Holm GH, Johnson EM, Maginnis MS, Naik S, Skelton WB, Wetzel JD, Wilson GJ, Chappell JD, Dermody TS. 2007. A plasmid-based reverse genetics system for animal double-stranded RNA viruses. *Cell Host Microbe* 1:147–157. <https://doi.org/10.1016/j.chom.2007.03.003>.